ARTICLE NO. 79-0109R

Transonic Sting Interference

L.E. Ericsson* and J.P. Reding†
Lockheed Missiles & Space Co., Inc., Sunnyvale, Calif.

One of the problems that has to be solved in order to improve the accuracy of the results obtained in ground facilities is that of support interference, especially in regard to dynamic test data. While the dynamic sting interference has been well documented for hypersonic flow, it is generally only expected at transonic speeds in the cases where the body has a bulbous, dome-shaped base or a boattail. However, it is shown in the present paper that when boundary-layer transition occurs on the aft body, sting interference becomes a problem for all body geometries.

Nomenclature

c = reference length = d_B
d = body diameter
l = total body length
l_0 = sharp cone length
M = Mach number
M_p = pitching moment: coefficient $C_m = M_p/(\rho_\infty U_\infty^2/2)\,Sc$
N = normal force: coefficient $C_N = N/(\rho_\infty U_\infty^2/2)S$
p = static pressure
q = pitch rate
Re = Reynolds number
$Re_{l\infty}$ = $l_\infty U_\infty/\nu_\infty$
S = reference area = $\pi c^2/4$
t = time
U = axial velocity
$\bar{U}$ = mean convection velocity
x = axial distance from nosetip
$\Delta\bar{x}$ = rotation center (Fig. 2)
α = angle of attack
$\Delta\alpha$ = oscillation amplitude
Δ = difference or increment
δ = angular sting deflection
θ = body perturbation in pitch
θ_c = cone half angle
ν = kinematic viscosity of air
ρ = air density

Subscripts

B = base
c.g. = center of gravity or oscillation center
d = downstream convection
i,I = interference
tr = transition
u = upstream convection (in wake)
W = wake neck
∞ = freestream value

Superscripts

i = induced, e.g. $\Delta^i C_{m\alpha}$

Derivative Symbols

$\dot{\alpha}$ = $\partial\alpha/\partial t$ $\quad C_{N\dot{\alpha}} = \partial C_N/\partial\alpha$
C_{mq} = $= \partial C_m/(\partial cq/U_\infty)$ $\quad C_{m\dot{\alpha}} = \partial C_m/\partial(c\dot{\alpha}/U_\infty)$
$C_{m\dot{\phi}}$ = $C_{mq} + C_{m\dot{\alpha}}$

Introduction

A REVIEW of the present state-of-the-art in wind-tunnel testing[1] has showed that the instrumentation acccuracy is no longer the pacing item in reaching the degree of precision that will be required for future aerodynamic designs. Rather, it is the quality of the flow in the test section and lack of accurate definition of interference effects from tunnel walls and model supports. Support interference presents a problem, especially in regard to dynamic test data. While the dynamic sting interference has been well documented for hypersonic flow,[2,3] it is generallly only expected at transonic speeds in the cases where the body has a bulbous base or a boattail.[3,4] it will be shown herein that when boundary-layer transition occurs on the aft body, sting interference becomes a problem for all geometries.

Statement of Problem

In Fig. 1, the pitch damping of a 12.5 deg sharp cone measured at $M_\infty = 1$ on a sting-supported model[5] and on a magnetically suspended half model[6] is compared with theory.[7,8] It can be seen that the data for the sting-supported model[5] deviate greatly from the theoretical data, until the data points are corrected for sting interference. How this correction is accomplished will be described.

The open unbarred data points in Fig. 1 are the results for $\alpha = 0$ in Fig. 2. The nonlinear variation with α of the pitch damping must be caused by viscous flow effects. Similar nonlinear behavior has been observed to be caused by sting interference (Fig. 3), but at transonic speeds, only when a bulbous base is present.[2,4] It has been suggested earlier[9] that the nonlinear behavior in Fig. 2 is caused by boundary-layer transition. Transition has been observed to cause a substantial increase of the pitch damping for typical center of gravity (c.g.) locations (giving static stability)[10] (Fig. 4), and the nonlinear effect is limited to small angles of attack (Fig. 5), all in agreement with the data trends in Fig. 2. The inset in Fig. 5 illustrates how the sting support can aggravate the transition movement in a dynamic test. Figure 6 shows the Reynolds number $Re_{l\infty}$ for the sharp and blunted cones tested by Wehrend.[5] Also shown is the transition Reynolds number measured on sharp cones in the 6×6 ft wind tunnel, (the tunnel in which Wehrend's experiment was performed) and in the 2×2 ft wind tunnel (the pilot tunnel for the 6×6 ft wind tunnel.)[11] The data strongly suggest that boundary-layer transition occurred on the aft body on the sharp cone but not on the blunted cone. Unfortunately, Wehrend investigated only the blunted cone to see if a cone with a flat base could

Presented as Paper 79-0109 at the 17th Aerospace Sciences Meeting, New Orleans, La., Jan. 15-17, 1979; submitted Feb. 12, 1979; revision received July 10, 1979.

Index categories: Jets, Wakes, and Viscid-Inviscid Flow Interactions; Nonsteady Aerodynamics; Transonic Flow.

*Consulting Engineer. Associate Fellow AIAA.
†Staff Engineer. Associate Fellow AIAA.

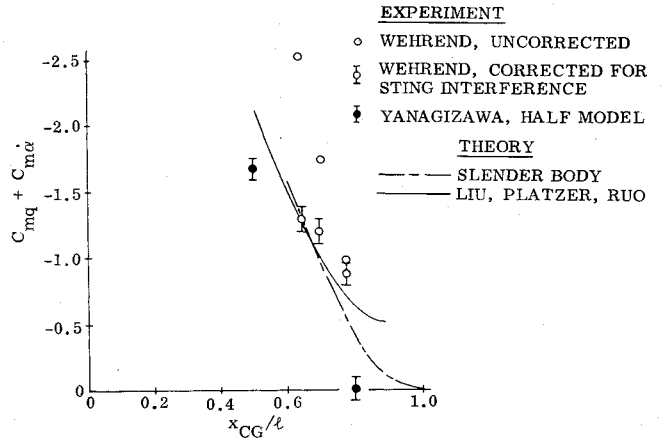

Fig. 1 Pitch damping of a 12.5 deg sharp cone at $M_\infty = 1$ for various rotation centers.

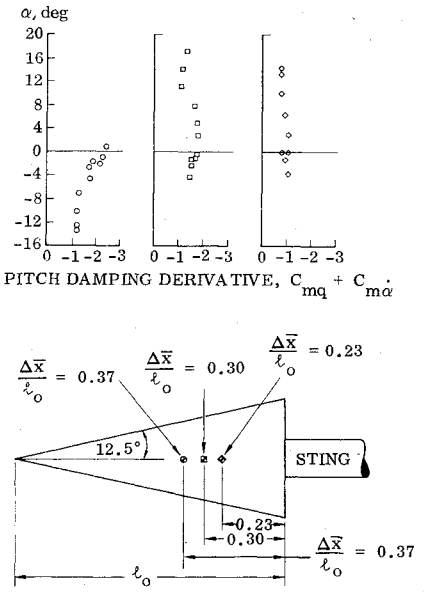

Fig. 2 Variation of pitch damping with angle-of-attack at $M_\infty = 1$ (sharp cone, Ref. 5).

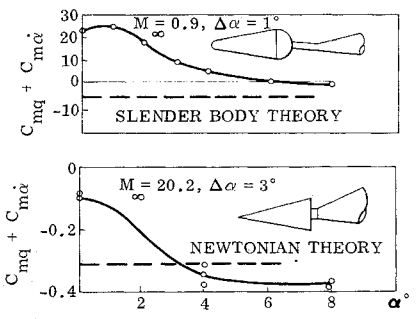

Fig. 3 Examples of nonlinear sting interference effects.[2]

also have sting interference. As is shown by Fig. 7 (compared with Fig. 2), the blunted cone does not exhibit the low-α nonlinearity.

Analysis

The nonlinear characteristics near $\alpha = 0$ in Fig. 2 are caused by the combined effects of boundary-layer transition and string interference. The question now is: How much would the transition effect be in the absence of sting interference? As

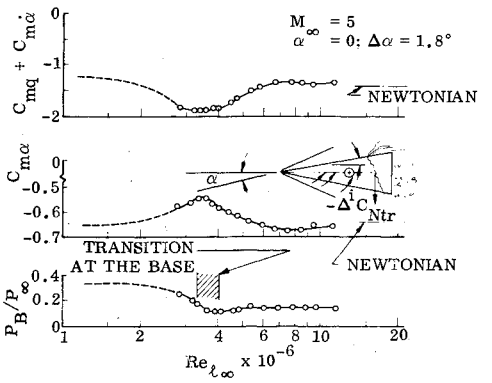

Fig. 4 Effect of boundary-layer transition on sharp cone aerodynamic characteristics.[10]

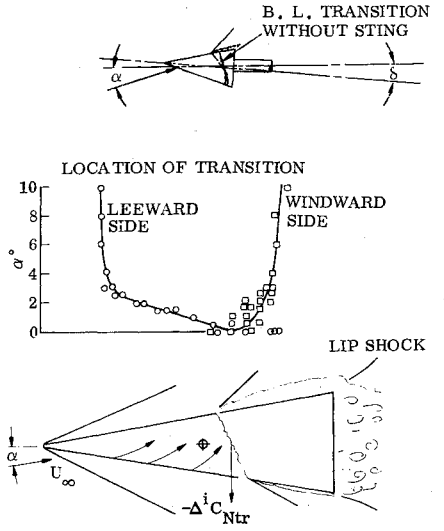

Fig. 5 Effect of angle-of-attack on transition front location at $Re_{l\infty} = 8 \times 10^6$ (Ref. 10).

both sting interference and transition effects are peaking at $\alpha = 0$, and both are restricted to a narrow α range around $\alpha = 0$ (compare Fig. 3 with Fig. 5), it is rather difficult to differentiate between the two effects. However, the analyses in Refs. 2 and 12 indicate that the time lag effects are very different in magnitude‡ for the two cases, being almost an order of magnitude larger for the sting interference effect than for the transition influence. Thus, it should be possible to differentiate between the two effects by investigating the relative dynamic and static stability effects.

The nonlinear contributions to $C_{m\theta} = C_{mq} + C_{m\dot{\alpha}}$ is defined as follows:

$$\Delta C_{m\theta} = (C_{m\theta})_{\alpha=0} - (C_{m\theta})_{\alpha>10\,\text{deg}} \tag{1}$$

where $(C_{m\theta})_{\alpha>10\ \text{deg}}$ is the level established by the experimental data for $10\ \text{deg} < \alpha < 20\ \text{deg}$.

From Ref. 12, one obtains the following expression for the dynamic amplification due to convective time lag of the transition-induced aerodynamics:

$$\frac{\Delta C_{m\dot{\theta}}}{\Delta C_{m\alpha}} = \frac{l}{c}\left[\left(\frac{x_i}{l} - \frac{x_{c.g.}}{l}\right) - \left(\frac{x_{tr}}{l} - \frac{x_i}{l}\right)\Big/\frac{\bar{U}}{U_\infty}\right] \tag{2}$$

‡They are otherwise similar, causing a reversal between static and dynamic effects. Thus, both the effect of transition and the cylindrical sting interference effect decrease static and increase dynamic stability (see Refs. 2 and 9 and Fig. 4).

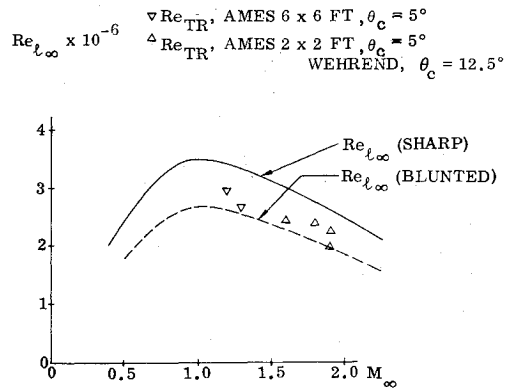

Fig. 6 Comparison of test and transition Reynolds numbers.

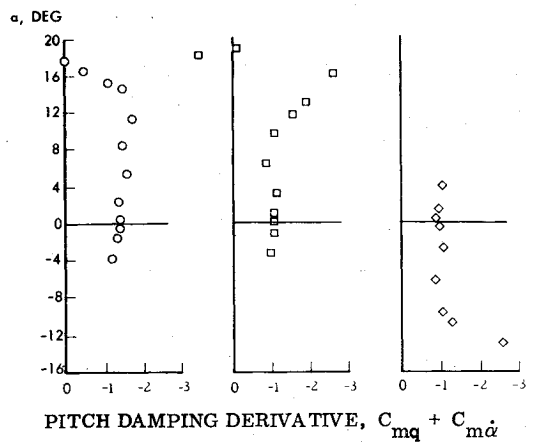

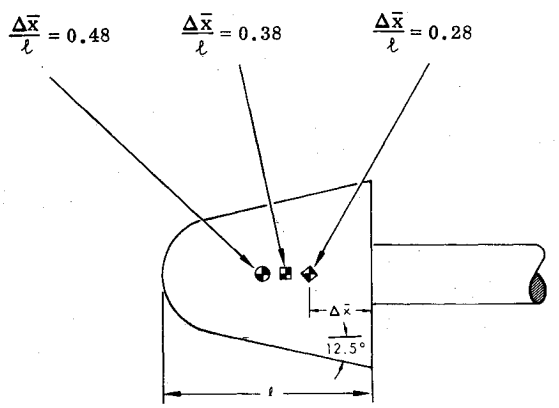

Fig. 7 Variation of pitch damping with angle-of-attack at $M_\infty = 1$ (30% blunt cone, Ref. 5).

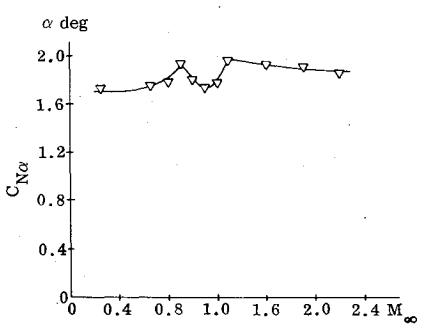

Fig. 8 $C_{N\alpha} = f(M_\infty)$ for a 12.5 deg sharp cone.[5]

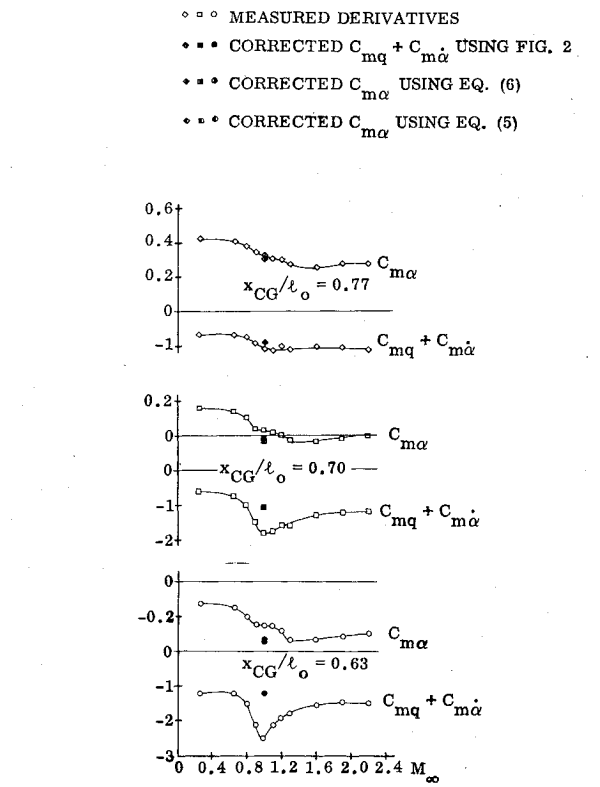

Fig. 9 Measured and corrected aerodynamic characteristics for a 12.5 deg sharp cone.

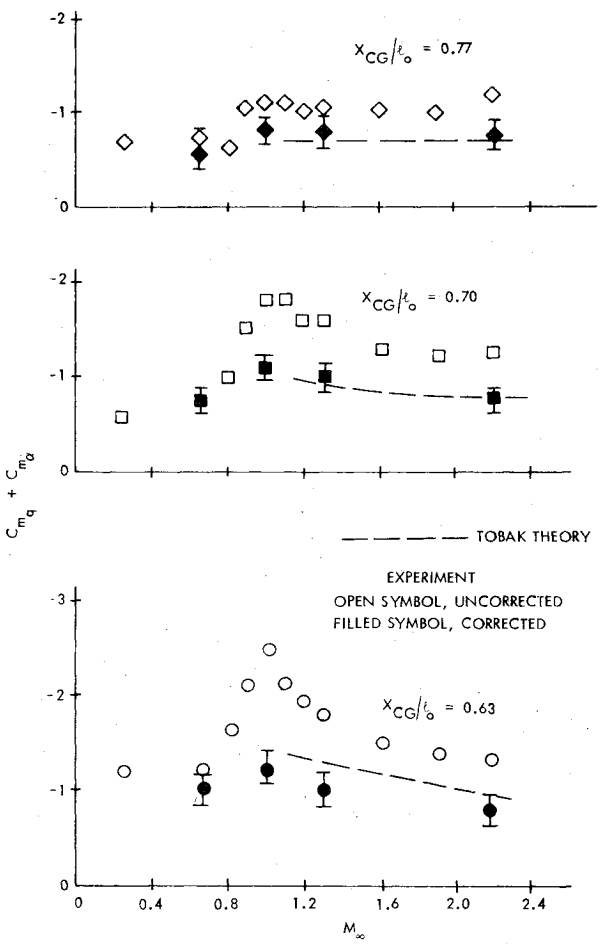

Fig. 10 Comparison between corrected damping measurements and theory.

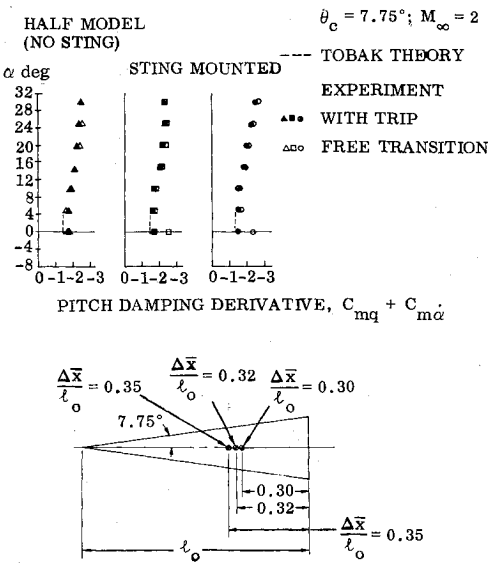

Fig. 11 Documentation of transition-amplified sting interference for a 7.75 deg sharp cone.[11]

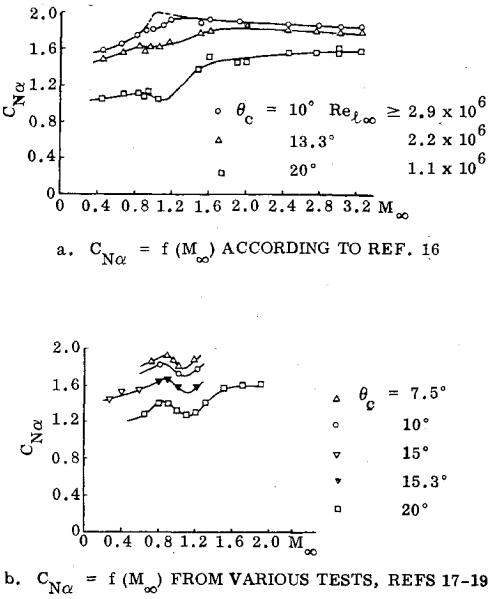

Fig. 12 $C_{N\alpha}$ as a function of Mach number for various sharp cones.

where $\bar{U}/U_\infty \approx 0.8$. With $x_i/l \geq 0$ and $x_{tr}/l < 1$, Eq. (2) gives

$$-\frac{\Delta C_{m\dot{\theta}}}{\Delta C_{m\alpha}} < \frac{l}{c}\left(\frac{x_{c.g.}}{l} + \frac{U_\infty}{\bar{U}}\right) \tag{3}$$

Thus, the largest amplification obtainable due to pure boundary-layer transition effects is 2.25 l/c, which for Wehrend's 12.5 deg cone is 5.

The amplification for the sting interference effect is defined by Ref. 2 as follows:

$$\frac{\Delta^i C_{m\delta}}{\Delta^i C_{m\delta}} = \frac{\Delta C_{m\dot{\theta}}}{\Delta C_{m\alpha}} = \frac{l}{c}\left[\frac{x_I}{l} - \frac{x_{c.g.}}{l} - \left(\frac{x_W}{l} - \frac{x_I}{l}\right)\left(\frac{U_\infty}{\bar{U}_d} + \frac{U_\infty}{\bar{U}_u}\right)\right] \tag{4}$$

where x_I/l is the location of the interference load ($x_I = x_{tr}$), x_W/l is the location of the wake stagnation point (the "wake neck"), and $\bar{U}_d$ and $\bar{U}_u$ respectively are the downstream and upstream communication velocities in the wake. Both Wehrend's own measurements[5] and recent sting interference measurements at supersonic speeds[13] indicate a critical sting length of 2 base diameters for flared sting interference. Thus, $x_W/l = 1 + 2\,c/l$. The wake downstream convection velocity in the free shear layer is assumed to be the same as for the boundary layer before "lift-off," i.e., $\bar{U}_d/U_\infty \approx 0.8$. For the upstream wake communication, the assumption of a small sting diameter[2] gives $\bar{U}_u/U_\infty \approx 0.2$. For the above parameter values, Eq. (4) becomes

$$\frac{\Delta^i C_{m\delta}}{\Delta^i C_{m\delta}} \approx \frac{l}{c}\left[\left(\frac{x_{tr}}{l} - \frac{x_{c.g.}}{l}\right) - 6.25\left(1 + 2\frac{c}{l} - \frac{x_{tr}}{l}\right)\right] \tag{5}$$

Equation (5) indicates that the dynamic amplification for the sting interference effect will be approximately 13.5 independently of the c.g. location. From Wehrend's measurements[5] (Fig. 8), one obtains $\Delta C_{N\alpha} = 0.20$ for $M_\infty = 1$. The sharp cone data in Fig. 6 give $x_{tr}/l \approx 0.80$. As the transition-induced static stability increment is

$$\Delta C_{m\alpha} = -\Delta C_{N\alpha}(x_{tr}/l - x_{c.g.}/l) \tag{6}$$

one obtains $\Delta C_{m\alpha} = 0.014$, 0.045, and 0.077, respectively, for the c.g. locations $x_{c.g.}/l = 0.77$, 0.70, and 0.63. From Fig. 2 the dynamic effects obtained for the same c.g. locations are $\Delta C_{m\dot{\theta}} = -0.30$, -0.70, and -1.25, respectively, giving the values $-\Delta C_{m\dot{\theta}}/\Delta C_{m\alpha} = 21.4$ 15.5, and 16.3 for the corresponding dynamic amplifications. Thus, it is clear that the nonlinear behavior at $\alpha = 0$ in Fig. 2 is mainly due to sting interference effects. Equation (5) gives the dynamic amplification values $\Delta^i C_{m\delta}/\Delta^i C_{m\delta} = 15.23$, 15.00, and 14.92 for the same three c.g. locations.

Discussion of Results

In Fig. 9 the dynamic derivative $C_{mq} + C_{m\dot{\alpha}}$ and the static derivative $C_{m\alpha}$ measured by Wehrend[5] for the three different c.g. locations are shown as functions of the Mach number. The solid corrected dynamic data points at $M_\infty = 1$ were obtained directly from Fig. 2. The corrected static stability derivative at $M_\infty = 1$ was obtained in two ways: 1) from Eq. (6) as discussed earlier, and 2) from Eq. (5) with

$$\Delta C_{m\alpha} = \Delta C_{m\dot{\theta}} \Big/ \left(\frac{\Delta^i C_{m\delta}}{\Delta^i C_{m\delta}}\right)$$

where $\Delta C_{m\dot{\theta}}$ is obtained from Fig. 2. It can be seen in Fig. 9 that the results obtained by these two independent methods are in very close agreement. Figure 1 shows that when Wehrend's damping data at $M_\infty = 1$ are corrected for sting interference in the manner just described, they agree rather well with slender body theory[7] and the linearized transonic theory by Liu et al.,[8] and are also in better agreement with (sting-interference-free) half-model data.[6] Wehrend's data trends indicate that transition-amplified sting interference was present throughout the supersonic speed region (Fig. 10). Orlik-Rückemann et al.[14] have documented the existence of transition-amplified sting interference for slender cones at $M_\infty = 2$ (see Fig. 11). For the sting-mounted model, the nonlinear increase of damping at $\alpha = 0$ was obtained with natural boundary-layer transition, but not for a tripped turbulent boundary layer. It is confirmed by the half-model data in Fig. 11 that it is the sting interference that dominates, as was deduced earlier from the dynamic amplification, because in this case the trip had no effect, and no nonlinearity was observed at $\alpha = 0$. That is, the effect of transition in the absence of sting interference is negligible at transonic and low supersonic speeds.

The corrected data in Fig. 10 agree well with the Tobak-Wehrend theory[15] for the two aft c.g. locations, but not so

well fo the forward c.g.,

$$x_{c.g.}/l_0 = 0.77$$

It is difficult to say to what extent this may be explained by the fact that the forward c.g. data were obtained in the opposite half of the wind tunnel, i.e., for negative rather than for positive angles of attack (see Fig. 2). In any case, much more detailed experimental data are needed before this transition-amplified sting interference can be defined better.

Conclusions

A review of the existing experiment data base for slender vehicle dynamics at transonic speeds has shown that when boundary-layer transition occurs on the aft body, a standard type sting support can greatly affect the measured aerodynamic damping. As much as 100% too-high damping can be indicated by the test results, provided that transition occurs at this critical near-base location. How common is this? According to Fig. 12, which shows all the experimental $C_{N\alpha}$ data for slender cones that the present authors could find,[16-19] it is very common. Consequently, the experimental data base for slender vehicle dynamics at transonic speeds has to be examined closely in regard to these unconservative sting interference effects.

References

[1] Whitefield, J.D., Hartin, J.P., and Pate, S.R., "Aerodynamic Testing – A Look at Future Requirements," AIAA Paper 78-765, AIAA 10th Aerodynamic Testing Conference, San Diego, Calif., April 1978.

[2] Reding, J.P. and Ericsson, L.E., "Dynamic Support Interference," *Journal of Spacecraft and Rockets,* Vol. 9, July 1972, pp. 547-553.

[3] Ericsson, L.E. and Reding, J.P., "Viscous Interaction or Support Interference – The Dynamicist's Dilemma," *AIAA Journal,* Vol. 16, April 1978, pp. 363-368.

[4] Ericsson, L.E. and Reding, J.P., "Aerodynamic Effects of Bulbous Bases," NASA CR-1339, Aug. 1969.

[5] Wehrend, W.R., Jr., "An Experimental Evaluation of Aerodynamic Damping Moments on Cones with Different Centers of Rotation," NASA TN D-1768, March 1963.

[6] Yanagizawa, M., "Measurement of Dynamic Stability Derivative of Cones and Delta-Wings at High Speeds," NAL TR-172, National Aerospace Lab., Tokyo, Japan, 1969.

[7] Bisplinghoff, R.L., Ashley, R., and Halfman, R.L., *Aeroelasticity,* Addison-Wesley, Cambridge, Mass., 1955.

[8] Liu, D.D., Platzer, M.F., and Ruo, S.Y., "On the Calculation of Static and Dynamic Stability Derivatives for Bodies of Revolution at Subsonic and Transonic Speeds," AIAA Paper 70-190, New York, Jan. 1970.

[9] Ericsson, L.E. and Reding, J.P., "Boundary Layer Transiton and Dynamic Sting Interference," *AIAA Journal,* Vol. 8, Oct. 1970, pp. 1886-1888.

[10] Ward, L.K., "Influence of Boundary-Layer Transition on Dynamic Stability at Hypersonic Speeds," *Transactions of the Second Technical Workshop on Dynamic Stability Testing,* Vol. II, Paper 9, 1965, Arnold Engineering Development Center, Tallahoma, Tenn.

[11] Ross, A.O., "Determination of Boundary Layer Transition Reynolds Numbers by Surface-Temperature Measurements of a 10° Cone in Various NACA Supersonic Wind Tunnels," NAA TN-3020, Oct. 1953.

[12] Ericsson, L.E., "Effect of Boundary Layer Transition on Vehicle Dynamics," *Journal of Spacecraft and Rockets,* Vol. 6, Dec. 1969, pp. 1404-1409.

[13] Uselton, B.L., "Sting Effects as Determined by the Measurement of Pitch-Damping Derivatives and Base Pressures at Mach 3," AIAA Paper 78-830, April 1978.

[14] Orlik-Rückemann, K.J., LaBerge, J.G., and Inyengar, S., "Half- and Full-Model Experiments on Slender Cones at Angle of Attack," *Journal of Spacecraft and Rockets,* Vol. 10, Sept. 1973, pp. 575-580.

[15] Tobak, M. and Wehrend, W.R., "Stability Derivatives of Cones at Supersonic Speeds," NACA TN 3788, Sept. 1956.

[16] Staff, Aeroballistics Division, NASA MSFC, "Aerodynamic Characteristics of Spherically Blunted Cones at Mach Numbers from 0.5 to 5.0," MTP-AERO-61-38, Huntsville, Ala., May 1962.

[17] Wehrend, W.R., Jr. and Reese, D.E., Jr., "Wind Tunnel Tests of the Static and Dynamic Stability Characteristics of Four Ballistic Re-entry Bodies," NASA TMX-369, June 1960.

[18] Kelly, T.C., "Investigation at Transonic Mach Numbers of the Effects of Configurational Geometry on Surface Pressure Distributions for a Simulated Launch Vehicle," NASA TM-X-845, Aug. 1963.

[19] Henderson, W.P., "Pressure Distributions Over the Forward Portion of the Project Fire Space Vehicle Configuration at Mach Numbers from 0.25 to 0.60," NASA TND-1612.